Generation of wavelength-tunable few-cycle pulses in the mid-infrared at repetition rates up to 10kHz

Sanari, Yasuyuki; Sekiguchi, Fumiya; Nakagawa, Kotaro; Ishii, Nobuhisa; Kanemitsu, Yoshihiko; Hirori, Hideki

Optics Letters

Generation of wavelength-tunable few-cycle pulses in the mid-infrared at repetition rates up to 10 kHz

Yasuyuki Sanari,[1] Fumiya Sekiguchi,[1] Kotaro Nakagawa,[1] Nobuhisa Ishii,[2,3] Yoshihiko Kanemitsu,[1,4] and Hideki Hirori[1,5]

[1]Institute for Chemical Research, Kyoto University, Uji, Kyoto 611-0011, Japan
[2]Kansai Photon Science Institute, National Institutes for Quantum Science and Technology (QST), Kizugawa, Kyoto 619-0215, Japan
[3]e-mail: ishii.nobuhisa@qst.go.jp
[4]e-mail: kanemitu@scl.kyoto-u.ac.jp
[5]e-mail: hirori@scl.kyoto-u.ac.jp

Received 12 August 2021; revised 10 September 2021; accepted 27 September 2021; posted 28 September 2021 (Doc. ID 440228); published 15 October 2021

We demonstrate a compact and tunable mid-infrared light source that provides carrier-envelope-phase (CEP)-locked pulses at repetition rates from 500 Hz to 10 kHz. The seed pulses were generated by intra-pulse difference frequency mixing of the output of an Yb:KGW regenerative amplifier that had been spectrally broadened by continuum generation using multiple plates. Then, a two-stage optical parametric amplifier was used to obtain output energies of about 100 μJ/pulse for center wavelengths between 2.8 and 3.5 μm. Owing to the intense pulse energies, it was possible to compress the multi-cycle pulses down to two-cycle pulses using YAG and Si plates.

https://doi.org/10.1364/OL.440228

Studies on light–matter interactions have profited greatly from recent advances in ultrashort pulse generation because extremely strong fields of ultrashort laser pulses can induce a variety of nonlinear phenomena in matter. One prominent example of these phenomena is high-order harmonic generation (HHG), where strong interaction between light and atoms or molecules beyond the perturbative regime results in emission of high-order harmonics of the fundamental light. HHG is indispensable for studies in the field of attosecond science as well as for coherent light sources in the x ray region [1–3]. Furthermore, intense ultrashort pulses with long wavelengths are attracting much attention in the field of light–matter interactions in solids because photon energies well below the bandgap of the material allow strongly light-driven processes without causing damage via real optical excitation. Long oscillation periods also result in an efficient acceleration of electrons in solids, i.e., an accumulation of the ponderomotive energy.

To date, light-induced exotic phenomena have been observed by strong excitation with terahertz pulses in the range from a few to several tens of terahertz [4–8]. In addition, optical pulses in the mid-infrared (MIR) region are also suitable for the investigation of extreme nonlinear phenomena because they can be tightly focused both in time and in space, resulting in ultrahigh electric fields. Because the duration of a single cycle of the electromagnetic field in this frequency region is shorter than the typical time constant of scattering processes in solids, such short pulses allow us to observe ultrafast coherent dynamics of electrons. For example, after the observation of HHG in ZnO [9], HHG in solids has been intensively investigated by using MIR pulses in order to elucidate possibilities for all-optical band-structure retrieval or compact x ray light sources [10–13]. To pursue such studies, further development of suitable light sources is indispensable.

Recently, optical parametric amplification of carrier-envelope-phase (CEP)-stabilized pulses has been demonstrated in the MIR region (around 3 μm). In particular, generation of extremely intense MIR light has been achieved [14–16], and it has been shown that high pulse energies allow us to reduce the pulse duration to a few cycles using nonlinear optical phenomena such as self-phase modulation [17–20]. Compared to multi-cycle pulses, such few-cycle optical pulses are advantageous for experiments on solids because a much higher electric field can be applied to the sample without causing optical damage (owing to their lower fluence) [21]. On the other hand, in order to perform precise spectroscopic measurements in the MIR region, light sources operating at high repetition rates have been developed [22–27]. To generate brighter high-order harmonics and to investigate the underlying nonlinear processes without damaging solids due to heat accumulation, an intense MIR light source with high tunability in terms of wavelength and repetition rate would be useful.

Here, we report on the development of a table-top MIR light source that combines the following four features: wavelength tunability, ultrashort pulses, a high CEP stability, and a tunable repetition rate in the range from sub-kHz to 10 kHz. For the seed pulse generation, the output of an Yb:KGW chirped-pulse amplifier was first spectrally broadened by fused-silica (FS) plates, and then these pulses were used for intra-pulse difference frequency generation (DFG). The obtained CEP-stable MIR

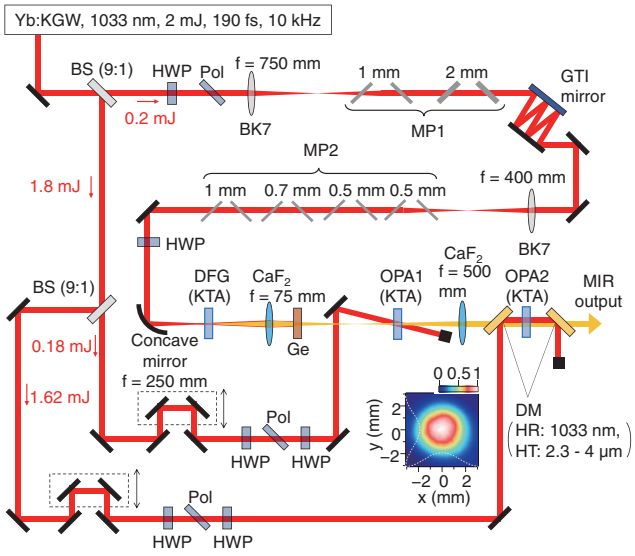

Fig. 1. Setup of the MIR light source. BS, beam splitter; HWP, half-wave plate; Pol, polarizer; MP1 and MP2, multi-plate compression stage 1 and 2; DFG, difference frequency generation; OPA1 and OPA2, optical parametric amplifier stage 1 and 2; MIR, mid-infrared; DM, dichroic mirror; HR, high reflectivity; HT, high transmittance. Inset, beam profile of the MIR output at a repetition rate of 10 kHz.

seed pulses were amplified in a $KTiOAsO_4$ (KTA)-based optical parametric amplifier (OPA). We confirmed that the center wavelength of the output pulses can be tuned from 2.8 to 3.5 μm and can have high pulse energies around 100 μJ/pulse. This high pulse energy obtained by the two-stage OPA allowed self-compression of the pulses using an yttrium aluminum garnet (YAG) plate. In the case of a center wavelength of 3.2 μm, the resulting CEP-stable MIR pulses had a pulse duration of 22 fs.

A schematic of the MIR pulse generation is shown in Fig. 1. The post self-compression stage is not included in this figure and is discussed separately. On the left upper side of Fig. 1, it is shown that the output of a commercial Yb:KGW laser (PHAROS PH2SP, Light Conversion; pulse energy 2 mJ, pulse duration 190 fs, center wavelength 1033 nm, repetition rate 10 kHz) was first split into two beams by a beam splitter (BS) (BS ratio 9:1). The repetition rate was changed by a pulse picker (Pockels cell) located before the BS (not shown in the figure). The beam with the smaller pulse energy of ≈ 0.2 mJ was used for the MIR seed generation. The other beam was split into a weak beam (0.18 mJ) and strong beam (1.62 mJ) for the pump pulses in the first and second stages of the two-stage OPA, respectively. The use of this multi-stage OPA has several advantages over pulse generation via a single stage only [28,29]. The advantages include the ability to compensate an angular chirp [28] and the robustness of the CEP owing to the collinear geometry, which does not require the beam locking with interferometric precision for spatially separated pump and signal beams used in DFG.

For the MIR seed generation, the pulses were focused by a lens ($f = 750$ mm) in front of the first stage of the multi-plate pulse compression (MP1). Here, the pulse energy was reduced to 170 μJ to avoid optical damage of the FS plates. MP1 is composed of two pairs of FS plates with different plate thicknesses (1 mm and 2 mm). The spectral bandwidth of the pulses is broadened by MP1 due to self-phase modulation. We aligned the FS plates in Brewster geometry in order to avoid surface reflection losses, and the use of paired plates minimizes aberration and chromatic dispersion. We compensated the dispersion by introducing three bounces on Gires–Tournois interferometer (GTI) mirrors and compressed the pulse duration for efficient spectral broadening at the second stage of the multi-plate pulse compression (MP2). The obtained compressed pulses were focused by a lens ($f = 400$ mm) in front of MP2. MP2 is composed of four pairs of FS plates with thicknesses of 0.5 mm, 0.5 mm, 0.7 mm, and 1 mm, respectively.

Figure 2(a) shows the spectrum before MP1 (black curve), and the spectra before (blue curve) and after MP2 (red curve). These spectra were measured for a repetition rate of 10 kHz, and we confirmed that the spectra were independent of the repetition rate. The short-wavelength (700–1100 nm) and long-wavelength (1100–1350 nm) regions of each spectrum were measured separately by two spectrometers (AFBR-S20M2WV, Broadcom and NIR-QUEST 512-2.5, Ocean Optics, respectively). After MP2, the pulses had an energy of 140 μJ and a significant spectral intensity in the wavelength region 800–1200 nm. The polarization of these pulses was rotated by 90 deg by a half-wave plate, and then the pulses were focused on a 2-mm-thick KTA crystal by a concave mirror ($f = 250$ mm). The intra-pulse DFG [e.g. 800 nm (o) subtracted by 1070 nm (e) leads to 3200 nm (o)] in the KTA crystal provided passively CEP-stabilized pulses with long wavelengths above 3000 nm. Then, the pulses passed through a Ge plate to select the wavelength region 3000–3500 nm for the MIR seed pulses. The obtained MIR seed pulses were amplified by a two-stage KTA-based OPA [1033 nm (o) → 1460–1640 nm (e) + 2800–3500 nm (o)]. For the first and second OPA stages (OPA1 and OPA2, respectively), we used KTA crystals with thicknesses of 3 mm and 4 mm, respectively. The lenses used to focus the seed pulses had focal lengths of $f = 75$ mm and 500 mm, respectively. The pump pulses for OPA2 were collinearly aligned with the seed pulses using a dichroic mirror (DM) with high reflectance at 1033 nm and high transmission in the MIR, and the generated MIR output beam was isolated from the pump pulses after OPA2 using another DM. The final beam profile of the MIR output is shown in the inset of Fig. 1; we obtained a Gaussian-like beam owing to the collinear OPA. The white dashed lines in the inset of Fig. 1 show the beam profiles in the horizontal (x) and vertical (y) directions. The ratio of the half-widths of these profiles at the positions corresponding to the $1/e$ - intensity, σ_x/σ_y, is 1.05 ± 0.02 at 10 kHz (almost the same was also obtained at 1 kHz).

The center wavelength of the MIR output can be tuned by changing the angles of the KTA crystals (for DFG and in OPA1 and OPA2). The tunability of the wavelength of the MIR output is analyzed in Figs. 2(b) and 2(c). The spectra in Fig. 2(c) were measured by a MIR spectrometer (MOZZA, Fastlite), and the pulse widths were determined by using second-harmonic generation frequency-resolved optical gating (SHG-FROG) based on a 400-μm-thick $AgGaS_2$ (AGS) crystal. Figure 2(b) specifies the correlation between the center wavelength and the pulse energy (red points) and the pulse duration (blue points). Overall, pulse energies larger than 80 μJ with temporal durations of about 100 fs [full width at half-maximum (FWHM)] were obtained for center wavelengths between 2.8 and 3.5 μm. The maximum achieved MIR pulse energy was 120 μJ at 3.0

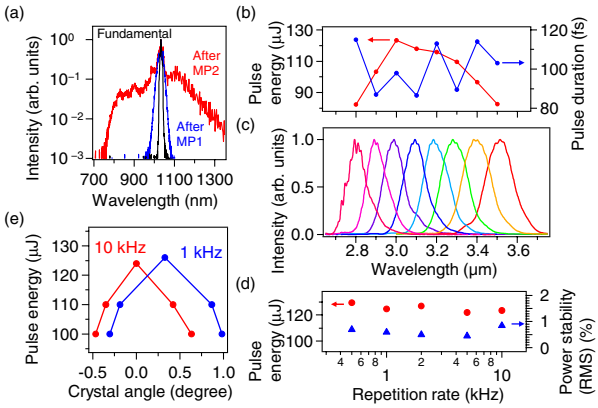

Fig. 2. (a) Spectra before and after MP1 and MP2. The spectra are normalized to their peak intensities. (b) Correlation between the center wavelength of the MIR output and the output pulse energy (red points) and the pulse duration (blue points). (c) Normalized amplitude spectra of the MIR output for different center wavelengths. (d) The repetition rate dependences of the output pulse energy at 3 μm and the power stability (RMS). (e) The dependence of the pulse energy on the angle of the KTA crystal of OPA2 for two different repetition rates.

μm, which corresponds to a quantum efficiency of about 17% (120 μJ/2000 μJ × 3000 nm/1033 nm).

We also investigated how the MIR pulse energy depends on the repetition rate of the Yb:KGW laser. Since the temperatures of the crystals in the system can change depending on the repetition rate of the Yb:KGW laser, their refractive indices can also change with the repetition rate. As the phase matching condition is determined by the refractive index, it is necessary to slightly modulate the crystal angles and the plate positions when the repetition rate is changed. Figure 2(d) shows the pulse energy and power stability measured by a thermal sensor with a response time of slightly less than 1 s (10 A, Ophir) as a function of the repetition rate. The output pulse energy shows no significant dependence on the repetition rate in the range from 500 Hz to 10 kHz. For all the repetition rates, the root mean square (RMS) error of the power was less than 0.9%. As shown in Fig. 2(e), the crystal angle should be slightly corrected if the repetition rate is changed. The difference between the optimum crystal angles may be a result of a larger temperature increase for 10 kHz because the larger refractive index of KTA at higher temperatures suggests a smaller optimum crystal angle. This result indicates that the pulse properties at higher repetition rates do not degrade strongly due to accumulated heat in the optical components. Therefore, this MIR light source can be operated at repetition rates up to 10 kHz with consistent pulse properties.

Now we discuss the pulse properties obtained by adding the post self-compression stage in Fig. 3(a) to the system in Fig. 1. As shown in Fig. 3(a), the output pulses from the two-stage OPA were further compressed by using multiple plates followed by dispersion compensation for the residual group-delay dispersion (GDD). Efficient self-compression of the output pulses in a dielectric is possible because our two-stage OPA provides a high pulse energy [20,30,31]. As in [20], we used a YAG plate and two Si plates to spectrally broaden the MIR pulses. A 2-mm-thick CaF_2 plate ($-266\ fs^2$ GDD) was inserted in the optical path to compensate the spectral dispersion induced in this post self-compression. Due to this post self-compression stage, the

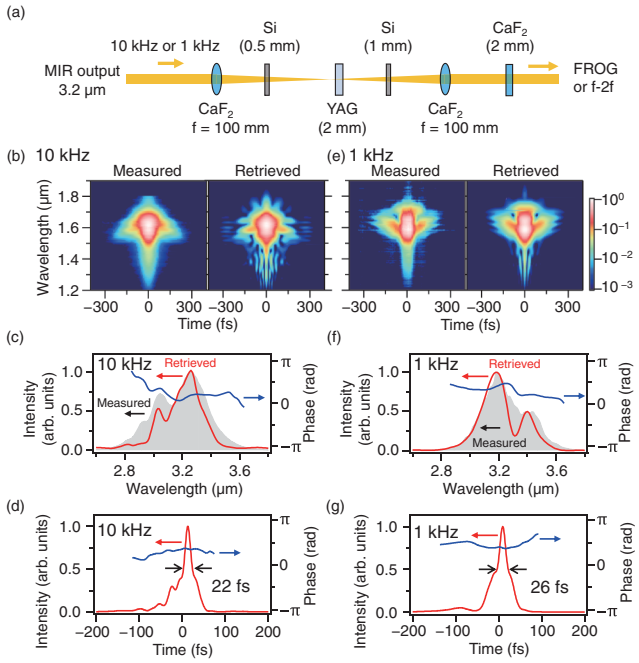

Fig. 3. (a) Experimental setup for pulse compression. (b) Measured (left panel) and retrieved (right panel) SHG-FROG traces for 10 kHz. (c) Measured spectrum (gray filled area) and the retrieved intensity (red curve) and phase (blue curve) spectra for 10 kHz. (d) Retrieved temporal profile (red curve) and phase (blue curve) for 10 kHz. The data for 1 kHz are shown in (e)–(g).

output pulse energy decreased from 110 μJ to 50 μJ. Figures 3(b)–3(d) show the SHG-FROG measurement results of the compressed MIR pulses with a center wavelength of 3.2 μm and at a repetition rate of 10 kHz. Figures 3(b) shows the measured (left panel) and retrieved (right panel) SHG-FROG traces. Figure 3(c) shows the retrieved intensity (red curve) and phase (blue curve) spectra and the spectrum measured by the MIR spectrometer (gray filled area). The experimental data and the calculations are in good agreement, and the phase is flat within the considered spectral range. The retrieved time traces of the spectral intensity and phase are shown in Fig. 3(d). A very short temporal duration of 22 fs (FWHM of the intensity) is obtained at 3.2 μm, which corresponds to a two-cycle pulse. Additionally, the same measurements were performed for a repetition rate of 1 kHz as shown in Figs. 3(e)–3(g). Figure 3(g) confirms that a compression to 26 fs (FWHM) can be achieved at 1 kHz. In contrast, in our previous work [27], the maximum output energy was limited to 60 μJ (at 6 kHz) because of the smaller pulse energy of the light source. Due to the smaller maximum output power, it was not possible to achieve self-compression.

Finally, to confirm the CEP stability of the MIR output pulses at a repetition rate of 10 kHz, we performed f-to-$2f$ interferometric measurements. Our experimental setup is shown in Fig. 4(a). First, we focused the compressed MIR pulses on a 1-mm-thick YAG plate by a CaF_2 lens ($f = 50$ mm) to expand the bandwidth further. The short-wavelength part of the obtained octave-spanning spectrum was combined with the second harmonic of the long-wavelength part generated in a 400-μm-thick AGS crystal using a wire-grid polarizer. The interference spectrum around 1.7 μm was measured by a MIR spectrometer (NIR-QUEST 512-2.5, Ocean Optics) with an

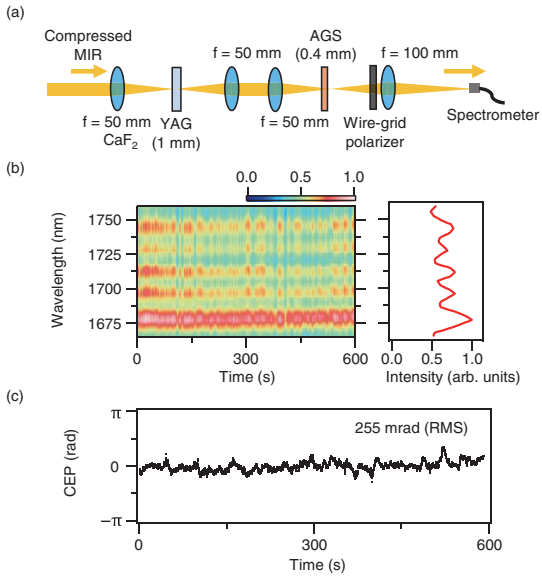

Fig. 4. (a) Experimental setup of the f-to-2f interference measurement. (b) Consecutively measured interference spectra (left panel), and a typical spectrum of the interference fringes (right panel). (c) 5000 CEP values measured during 600 s.

acquisition time of 1 ms. The measurement was repeated for 600 s (5000 acquisitions). The left panel of Fig. 4(b) shows a part of the recorded sequence of the interference fringes, and the right panel shows a single interference spectrum as example. The CEP values extracted from the interference spectra are plotted in Fig. 4(c), which evidences a stability of 255 mrad (RMS) over 600 s.

In conclusion, we have demonstrated a CEP-stable ultrafast MIR light source with a tunable wavelength range of 2.8–3.5 μm. This system can be operated with a high repetition rate of 10 kHz. The intense pulses (pulse energy of about 100 μJ) generated by the two-stage KTA-based OPA allowed us to compress the pulse down to a duration of 22 fs at 3.2 μm, which was determined by SHG-FROG measurements using an AGS crystal. The long-term CEP stability was confirmed by f-to-2f interference measurements. We have also shown that the pulse properties hardly change when the system is operated at different repetition rates in the range from 500 Hz to 10 kHz. This MIR light source, which provides ultrashort pulses and a variable repetition rate, will facilitate precise investigations of non-perturbative optical phenomena in solids.

Funding. Japan Society for the Promotion of Science (JP19H05465).

Disclosures. The authors declare no conflicts of interest.

Data Availability. Data underlying the results presented in this Letter are not publicly available at this time but may be obtained from the authors upon reasonable request.

REFERENCES

1. A. McPherson, G. Gibson, H. Jara, U. Johann, T. S. Luk, I. A. McIntyre, K. Boyer, and C. K. Rhodes, J. Opt. Soc. Am. B **4**, 595 (1987).
2. M. Ferray, A. L'Huillier, X. F. Li, L. A. Lompre, G. Mainfray, and C. Manus, J. Phys. B **21**, L31 (1988).
3. T. Ditmire, T. Donnelly, R. W. Falcone, and M. D. Perry, Phys. Rev. Lett. **75**, 3122 (1995).
4. K. Reimann, R. P. Smith, A. M. Weiner, T. Elsaesser, and M. Woerner, Opt. Lett. **28**, 471 (2003).
5. A. Sell, A. Leitenstorfer, and R. Huber, Opt. Lett. **33**, 2767 (2008).
6. H. Hirori, A. Doi, F. Blanchard, and K. Tanaka, Appl. Phys. Lett. **98**, 91106 (2011).
7. H. Hirori, K. Shinokita, M. Shirai, S. Tani, Y. Kadoya, and K. Tanaka, Nat. Commun. **2**, 594 (2011).
8. F. Sekiguchi, H. Hirori, G. Yumoto, A. Shimazaki, T. Nakamura, A. Wakamiya, and Y. Kanemitsu, Phys. Rev. Lett. **126**, 077401 (2021).
9. S. Ghimire, A. D. DiChiara, E. Sistrunk, P. Agostini, L. F. DiMauro, and D. A. Reis, Nat. Phys. **7**, 138 (2011).
10. O. Schubert, M. Hohenleutner, F. Langer, B. Urbanek, C. Lange, U. Huttner, D. Golde, T. Meier, M. Kira, S. W. Koch, and R. Huber, Nat. Photonics **8**, 119 (2014).
11. C. Schmidt, J. Bühler, A.-C. Heinrich, J. Allerbeck, R. Podzimski, D. Berghoff, T. Meier, W. G. Schmidt, C. Reichl, W. Wegscheider, D. Brida, and A. Leitenstorfer, Nat. Commun. **9**, 2890 (2018).
12. Y. Sanari, T. Otobe, Y. Kanemitsu, and H. Hirori, Nat. Commun. **11**, 3069 (2020).
13. Y. Sanari, H. Hirori, T. Aharen, H. Tahara, Y. Shinohara, K. L. Ishikawa, T. Otobe, P. Xia, N. Ishii, J. Itatani, S. A. Sato, and Y. Kanemitsu, Phys. Rev. B **102**, 041125 (2020).
14. G. Andriukaitis, T. Balciūnas, S. Ališauskas, A. Pugžlys, A. Baltuška, T. Popmintchev, M.-C. Chen, M. M. Murnane, and H. C. Kapteyn, Opt. Lett. **36**, 2755 (2011).
15. M. Bridger, O. Naranjo-Montoya, A. Tarasevitch, and U. Bovensiepen, Opt. Express **27**, 31330 (2019).
16. M. Musheghyan, P. P. Geetha, D. Faccialà, A. Pusala, G. Crippa, A. Campolo, A. G. Ciriolo, M. Devetta, A. Assion, and C. Manzoni, J. Phys B **53**, 185402 (2020).
17. D. Brida, M. Marangoni, C. Manzoni, S. De Silvestri, and G. Cerullo, Opt. Lett. **33**, 2901 (2008).
18. G. Fan, T. Balčiūnas, T. Kanai, T. Flöry, G. Andriukaitis, B. E. Schmidt, F. Légaré, and A. Baltuška, Optica **3**, 1308 (2016).
19. U. Elu, M. Baudisch, H. Pires, F. Tani, M. H. Frosz, F. Köttig, A. Ermolov, P. St.J. Russell, and J. Biegert, Optica **4**, 1024 (2017).
20. F. Lu, P. Xia, Y. Matsumoto, T. Kanai, N. Ishii, and J. Itatani, Opt. Lett. **43**, 2720 (2018).
21. T. T. Luu, M. Garg, S. Y. Kruchinin, A. Moulet, M. T. Hassan, and E. Goulielmakis, Nature **521**, 498 (2015).
22. M. Bradler, C. Homann, and E. Riedle, Opt. Lett. **36**, 4212 (2011).
23. K. Kaneshima, N. Ishii, K. Takeuchi, and J. Itatani, Opt. Express **24**, 8660 (2016).
24. N. Thiré, R. Maksimenka, B. Kiss, C. Ferchaud, P. Bizouard, E. Cormier, K. Osvay, and N. Forget, Opt. Express **25**, 1505 (2017).
25. M. Knorr, J. Raab, M. Tauer, P. Merkl, D. Peller, E. Wittmann, E. Riedle, C. Lange, and R. Huber, Opt. Lett. **42**, 4367 (2017).
26. M. Mero, Z. Heiner, V. Petrov, H. Rottke, F. Branchi, G. M. Thomas, and M. J. J. Vrakking, Opt. Lett. **43**, 5246 (2018).
27. N. Ishii, P. Xia, T. Kanai, and J. Itatani, Opt. Express **27**, 11447 (2019).
28. H. He, Z. Wang, C. Hu, J. Jiang, S. Qin, P. He, N. Zhang, P. Yang, Z. Li, and Z. Wei, Appl. Phys. B **124**, 31 (2018).
29. Z. Heiner, V. Petrov, G. Steinmeyer, M. Vrakking, and M. Mero, Opt. Express **26**, 25793 (2018).
30. M. Hemmer, M. Baudisch, A. Thai, A. Couairon, and J. Biegert, Opt. Lett. **21**, 28095 (2013).
31. V. Shumakova, P. Malevich, S. Ališauskas, A. Voronin, A. M. Zheltikov, D. Faccio, D. Kartashov, A. Baltuška, and A. Pugžlys, Nat. Commun. **7**, 12877 (2016).